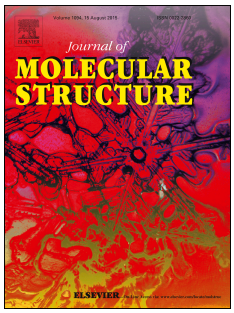

Theoretical investigation on the crystal structure, spectral and optical properties of a novel organic optical material: (Acetoxy) (2-methylphenyl) methylacetate

N. Sivakumar, J. Kanchanadevi, M. Govindarajan, R. Jayavel, G. Anbalagan

PII: S0022-2860(20)30904-2

DOI: https://doi.org/10.1016/j.molstruc.2020.128579

Reference: MOLSTR 128579

To appear in: *Journal of Molecular Structure*

Received Date: 6 February 2020

Revised Date: 11 May 2020

Accepted Date: 31 May 2020

Please cite this article as: N. Sivakumar, J. Kanchanadevi, M. Govindarajan, R. Jayavel, G. Anbalagan, Theoretical investigation on the crystal structure, spectral and optical properties of a novel organic optical material: (Acetoxy) (2-methylphenyl) methylacetate, *Journal of Molecular Structure* (2020), doi: https://doi.org/10.1016/j.molstruc.2020.128579.

From

Dr.N. Sivakumar,
UGC-Postdoctoral Fellow,
Crystal Growth Centre,
Anna University, Chennai-25
nsivakumar1986@gmail.com

To

The Editor
Journal of Molecular Structure,
Elsevier Publishing Company.

Respected Sir,

Sub: Research article Credit statement–reg.

I hereby stating that the article entitled "**Theoretical investigation on the crystal structure, spectral and optical properties of a novel organic optical material: (Acetoxy) (2-methylphenyl) methylacetate**" submitted for the publication in Journal of Molecular Structure is the original, and has been written by the stated authors who are all aware of its content and approve its submission.

The credits to the authours in the present research work is as follows,

N. Sivakumar : Characterization and Investigation
J. Kanchanadevi : Synthesis and solved the structure
M. Govindarajan : Vibrational analysis
G. Anbalagan : Validation of the research work
R. Jayavel: Review and editing.

Thanking You,
Yours Sincerely,
Dr. N. Sivakumar

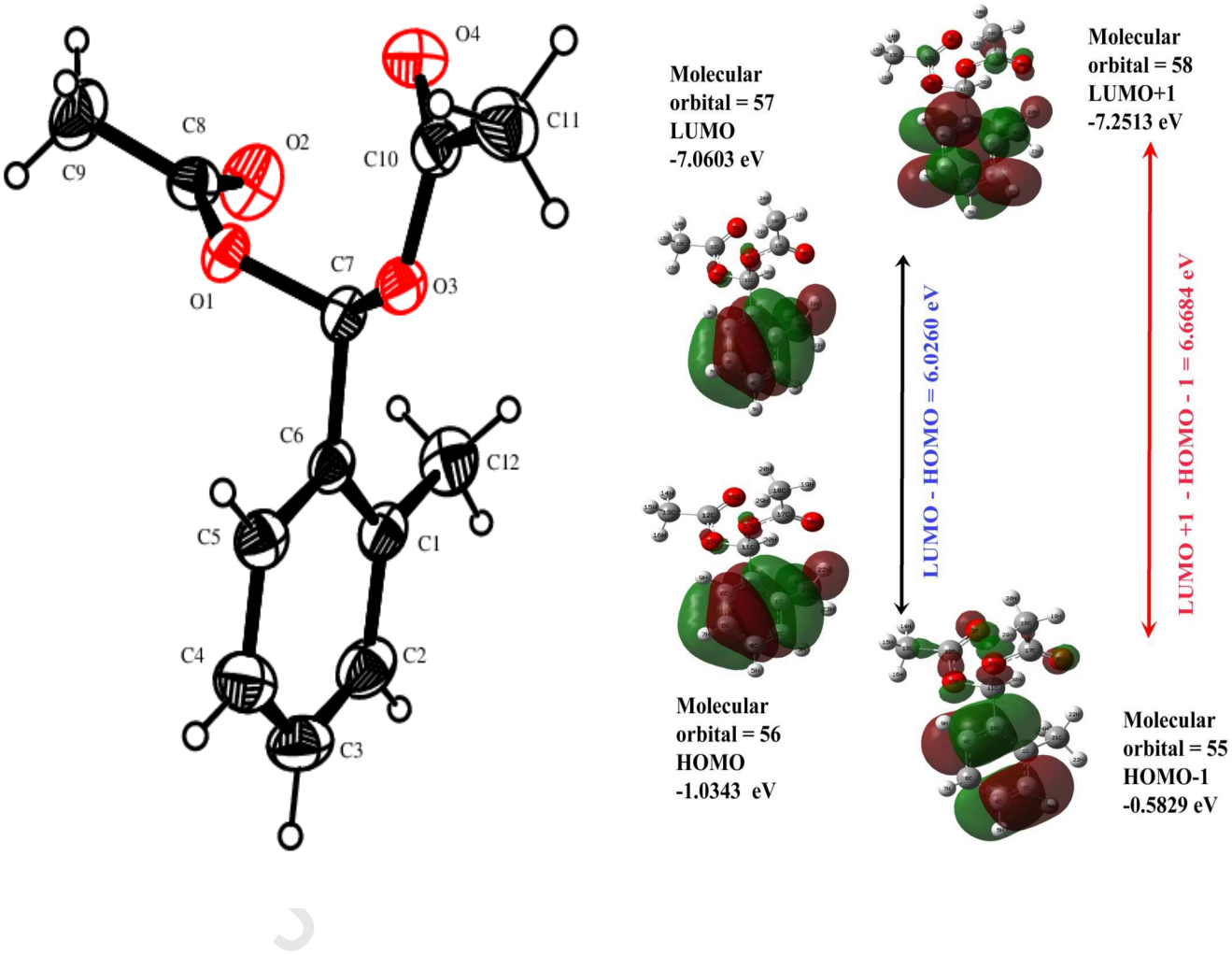
O4
C8
O2
C11
C9
C10
C7
O3
O1
C6
C12
C5
C1
C4
C2
C3
Molecular orbital = 57 LUMO -7.0603 eV
Molecular orbital = 58 LUMO+1 -7.2513 eV
LUMO - HOMO = 6.0260 eV
LUMO +1 - HOMO - 1 = 6.6684 eV
Molecular orbital = 56 HOMO -1.0343 eV
Molecular orbital = 55 HOMO-1 -0.5829 eV

Theoretical investigation on the crystal structure, spectral and optical properties of a novel organic optical material: (Acetoxy) (2-methylphenyl) methylacetate

N. Sivakumar[a,b*], J. Kanchanadevi[c], M. Govindarajan[d], R. Jayavel[a], G. Anbalagan[e,]**

[a]Crystal Growth Centre, Anna University, Chennai-600 025, India.

[b]Department of Physics, Saveetha Schoolo of Engineering, Saveetha University, Chennai-602 105

[b]Department of Physics, Presidency College, Chennai-600 005

[c]Bharathidasan Government College for Women, Puducherry-605 003, India.

[d]Department of Nuclear Physics, University of Madras, Chennai-600 005, India.

Corresponding Authors : *Dr. N. Sivakumar (E-mail: nsivakumar1986@gmail.com) and

**Dr. G. Anbalagn (E-mail: anbu24663@yahoo.co.in)

Abstract

An organic material (Acetoxy)(2-methylphenyl) methyl acetate (AMPMA) was synthesized at temperature and its chemical structure was analyzed by vibrational spectroscopic studies (FT-IR/FT-Raman) and NMR spectroscopy. HF and DFT/B3LYP theoretical methods were employed on AMPMA to investigate its molecular geometry, vibrational and bonding nature. The time-dependent HOMO-LUMO energy was found to be 6.0260 eV. The optical properties of the material were discussed through dipole moment and optical polarization. In this contest, the estimation of molecular dipole moment (μ) and linear polarizability (α) were studied by MP2, DFT and HF methods with different basis sets.

Keywords: Optical properties; Crystal structure; Molecular Geometry; Vibrational analysis; Energy gap.

1. Introduction

In recent ages, the synthesis of acylals has been of great research because of its wide variety of applications. The protecting groups are very much important in the synthesis of organic materials and are being a key factor in the development of many synthetic materials [1]. The 1,1-Diacetates are useful materials in asymmetric allylic alkylation, synthesis of natural products, and synthesis of 1-acetoxy dienes and 2,2-dichlorovinyl acetates in Diels-Alder reactions [2, 3]. The acylal functions could be altered to other groups with appropriate nucleophiles [4, 5] and 1,1-diacetates are the cross-linking agents for the cellulose in cotton and as bleaching initiators in wine-stained fabrics [6, 7]. (Acetoxy)(2-methylphenyl) methyl acetate (AMPMA) is an acylal-organic material. Acrylals are 1,1diacetates which has a general structure R-C(OOCR)$_2$, (where R represents an aromatic or aliphatic compound). The crystal structure of the title compound was reported and in which acetoxy groups are oriented with the benzene ring with an angle of 62.71 (6)° and 57.92 (5)° [8]. Centrosymmetric dimer has been developed via an R22(16) ring motif by the intermolecular C—H…O interaction with two acetoxy groups. Shirin and Khaligh conducted the acetylation of various alcohols, thiols, phenols, aldehydes and amines with acetic anhydride under solvent-free conditions in the presence of a catalyst-succinimide-N-sulfonic acid [9]. Most of the researchers concentrated only on the synthesis methods of acylals using different catalysts [1-10].

Organic crystal, (Acetoxy) (2-methylphenyl) methylacetate is a newly syntheisized material through the solvent evaporation method. In this material, there is a high degree of electron delocalization in the benzene rings which are optically sensitive and show a fast optical response. Therefore such kinds of organic materials are highly polarizable and show an excellent nonlinearity. In the present research work, the very first time we are reporting the

physiochemical properties of the (Acetoxy) (2-methylphenyl) methylacetate material through the chemical computational techniques to understand the details of various spectroscopic vibrations, electronic properties like HOMO-LUMO energies, electrostatic potential, thermodynamic and optical activities. Thus the properties explain the novelty or the originality of the titled material in the forthcoming sections.

2. Experimental

The precursor material, 2-methylbenzaldehyde and anhydrous indium bromide were taken in the 1:1 molar ratio. Initially, 2-methylbenzaldehyde was completely dissolved in 25 ml of acetic anhydride and indium bromide was gently added to the solution at room temperature. The obtained mixture was stirred under a nitrogen atmosphere for 4 hours to get a homogenous mixture. The product was washed well with the water and recrystallization processes were done with methanol solvent to get a pure final product with a yield of 82%.

3. Characterization

A Bruker kappa APEX II crystal X-ray diffractometer was used to collect the single crystal data of AMPMA crystal. A defect-free single crystal (0.30 ×0.20 × 0.20 mm^3) was selected and X-ray diffraction data were recorded at 293 K on a three-circle X-ray diffractometer fitted with Mo-Kα radiation of wavelength λ = 0.71073 Å. The ω: 2θ scan method was utilized to obtained reflections. The data were rectified for absorption and polarization effects with an empirical correction. The crystal structure of AMPMA was solved by SHELXL-97 method and deposited at the Cambridge Crystallographic Data Centre (CCDC No. 841279). The data was well-refined with full matrix (SHELXL-97) least square process by retaining 1856 reflections which satisfy the condition, $I > 2\sigma(I)$. The results of consecutive refinements on F^2 reveals the

low-reliability factor, R = 0.041 which reveals that the structure is more stable. The title crystal belongs to the Monoclinic system with the centrosymmetric space group of *C2/c*. The unit cell values were found to be a = 15.757(5)Å, b = 7.564(5)Å, c = 19.886(5)Å, β = 99.15(5)Å and V = 2339.8(18) Å^3.

Powder X-ray diffraction study was carried out on the titled crystal using XPERT-PRO equipment with Cu-Kα radiation of wavelength, 1.5406 Å. The XRD data were recorded in the Bragg angle (2θ) range from 5 to 50□ with a step size of 0.02/sec. The IR spectrum was obtained in the wavenumber region (4000- 400 cm^{-1}) with the help of the Perkin Elmer spectrum one FT-IR spectrometer (of resolution 0.5 cm^{-1}) using KBr pellet method. Raman spectral analysis was done in the range 3500-50 cm^{-1} with 500 scans using FT-Raman Bruker RFS 27:S Raman module (of resolution 2 cm^{-1}). Nd: YAG laser (1064 nm) with o/p power of 100 mW (air-cooled diode pumped) was used in the Raman spectral equipment. Both IR and Raman identifies the various chemical groups existing in the material. Further, the molecular structure was confirmed by NMR spectra recorded at 22°C using Bruker Advance III 500 MHz spectrometer with $CDCl_3$ as a solvent.

3.1. Quantum chemical calculations

Quantum chemical computations were performed at DFT (B3LYP) and ab-initio HF methods with Gaussian 09 program [11]. The vibrational frequencies at the various theoretical level and different basis sets with Cs point symmetry were calculated. In the optimized geometry, all the modes are real frequency modes and thus a minimum potential energy surface has been established on the molecule.

As a result, reduced masses, the unscaled estimated frequencies, force constants, depolarization ratios, IR/Raman intensities and Raman activities were calculated. In this

estimation, a uniform scaling factor was applied to balance the systematic faults initiated by vibrational anharmonicity, basis set incompleteness and neglect of electron correlation. Hence, the calculation on vibrational frequencies at the HF level is scaled to 0.905 [12]. For B3LYP/6-311++G(d,p), the wavenumbers above 1700 cm^{-1} are scaled with 0.958 and below 1700 cm^{-1} are scaled with 0.983 [13, 14]. The visual animation and the normal mode assignments were verified with the Gauss view program [15, 16]. DFT approach with B3LYP/6-311++G(d,p) level was employed to obtain the simulated electronic absorption spectra. The investigation of reactive sites of AMPMA was studied with MEP (molecular electrostatic potential) map. Moreover, the thermodynamic parameters like heat capacity, entropy and enthalpy were examined from vibrational frequency calculations at different temperatures.

3. 2. Calculation of Raman intensities

According to Raman scattering intensity theory, the calculated Raman activities (S_{Ra}) from the Gaussian 09 program can be transformed into relative Raman intensities (I_{Ra}) by the equation [17, 18]

$$I_i = \frac{f\left(\nu_0 - \nu_i\right)^4 S_i}{\nu_i\left[1 - \exp\left(-hc\nu_i / kT\right)\right]}$$

where, v_0 is the exciting wavenumber in cm^{-1} (here, v_0 = 9398.5 cm^{-1} and their corresponding wavelength is 1064 nm), v_i is the i^{th} vibrational wavenumber in cm^{-1}, S_i is the normal mode Raman scattering activity and $f(=10^{-12})$ is a constant normalization factor. Other symbols like *h*, *k*, *c* and *T* are representing their usual meaning.

4. Results and discussion

4.1. X-ray diffraction analysis

From the single crystal X-ray diffraction analysis, it is confirmed that the AMPMA crystal belongs to the monoclinic crystal system having a space group of C2/c. The crystallographic data and their optimized geometrical parameters are given in Table 1 and Table **SM 1 (Supplementary Material)** respectively. Table 2 provides information about an intermolecular hydrogen bond in the AMPMA single crystal. ORTEP diagram (Fig. 1) shows an intermolecular C—H···O interaction connecting acetoxy groups which develop a centrosymmetric dimer. The recorded powder X-ray diffraction pattern of the AMPMA crystal was compared with the simulated XRD pattern and is presented in Fig. 2. The simulated XRD pattern was obtained from Mercury software (version 3.7) by using the CIF file. It is observed from the XRD pattern that almost all the peak positions well coincided with the simulated spectrum and thus confirms the single monoclinic phase of the titled crystal.

4.2. Equilibrium geometry

Fig. 3 represents the optimized structure of the title molecule with *B3LYP/6-311++G(d,p)*. The global minimum energy and dipole moment of AMPMA were -766.8586 Hartrees and 2.8170 Debye respectively. The value of ZPVE called zero-point vibrational energy is estimated to be 150.3561 kcal mol^{-1}. The elongation and contraction of bond lengths and bond angles with the applied electric field would be responsible for the large polarizability of AMPMA. For the title molecule, the calculated and investigational bond length values of C1–C2 and C1–C10 are 1.392 and 1.389 Å, respectively (Table **SM 1**). It is greater than other bond lengths of C-C, in the benzene ring. The substitution of two methyl acetate groups to a toluene ring is liable for the elongation of C1–C2 and contraction of C1–C10 bonds. C12-O26 and C17-

O28 bonds are not much deviated in the methyl acetate. There are four C-O bond lengths, in which the bonds C11-O25 and C11-O27 are elongated more than the other two C12-O25 and C17-O27 bond lengths. The bond angle (C1–C10–C11= 121°) of elongation and (C8–C10–C11= 118°) of contraction from the benzene ring angle of 120° show the substitution effect in the ring. The acetic groups attached (C–C=O=125°) to the ring almost agreement with experimental values. The calculated and experimental bond lengths of AMPMA can be understood from the correlation graph which is given in Fig. **SM 1 (Supplementary Material)**. The calculations show good linear behavior of both the theoretical and investigational bond length values [8].

4.3. Vibrational analysis

Vibrational spectra are helpful to elucidate the role of H-bonds in the molecular structure displaying nonlinear optical activity in the crystal. The vibrational band assignments of theoretical and experimental wavenumbers of AMPMA are listed in Table **SM 2 (Supplementary Material)**. Vibrations that are present in both Raman and infrared spectrum are active. The experimental and computer-generated FT-IR and that of FT-Raman spectra of AMPMA are shown in Figs. 4 and 5 respectively.

4.3.1. Aromatic C-H vibrations

The aromatic compound reveals C-H stretching, C-H in-plane and C-H out-of-plane bending vibrations. C-H stretching vibrations of the aromatic compounds display multiple frail bands in wavenumber range 3100 to 3000 cm^{-1} [19]. In the current study, AMPMA is a mono switched aromatic system which describes the above three types of C-H stretching vibrations.

The C-H stretching vibration of AMPMA in the FTIR is observed at 3053 cm^{-1} and in the FT-Raman at 3065 cm^{-1}. This mode is estimated in the range 3068-3043 cm^{-1} with *B3LYP/6-311++G(d,p)*. HF method estimated in the C-H stretching vibrations in the range 3053-3013 cm^{-}

[1]. All bands have medium and strong intensities and were found in the predictable region.

The C-H in-plane bending vibrational bands are commonly noted in the region 1000 to 1300 cm^{-1} [20]. The in-plane bending vibrations are observed at 1135 cm^{-1} in FT-Raman and 1119 cm^{-1} in infrared. The theoretical vibrations well coincide with the experimental data.

The out-of-plane bending mode vibrations of C-H appears within the limit, 1000-700 cm^{-1} [21]. The vibrations identified at 735, 710, 650 and 618 cm^{-1} are allocated to C-H out-of-plane bending vibrations of AMPMA. These modes were computed at 743, 712, 647 and 618 cm^{-1} by the *B3LYP/6-311++G(d,p)* method and at 764, 730, 661 and 633 cm^{-1} by *HF/6-311++g(d,p)*. These changes in vibrations confirm the complex formation.

4.3.2. C-C vibrations

The C-C bands are more influential on aromatic ring modes. The aromatic ring C=C stretching modes generally present in the region, 1430–1625 cm^{-1} [22]. The stretching vibrations of C-C in an aromatic ring are anticipated within the wavenumber 1300-1000 cm^{-1} [23, 24].

The maximum ring modes are changed by the substitution to the aromatic ring. In the present molecule, the IR peak observed at 1588 cm^{-1} and Raman assignments at 1554 and 1468 cm^{-1} are attributed to C=C stretching mode of vibrations. These bands are estimated as 1624 cm^{-1} in DFT and 1582 cm^{-1} in HF methods. The vibrations identified at 1265 & 1155 cm^{-1} in FT-Raman and 1260 cm^{-1} in infrared are attributed to C-C vibrations. The corresponding bands are calculated at 1281 and 1265 cm^{-1} by HF and DFT methods respectively.

The C–C–C aromatic cycle vibrations are noticed in the predictable region 750-1000 cm^{-1} [25]. Experimental IR bands observed at 845 and 770 cm^{-1} and Raman band at 828 cm^{-1} are due to aromatic cycle vibrations. These bands have appeared at 927, 847, 824 and 768 cm^{-1} in DFT and 971, 881, 830 and 775 cm^{-1} in HF respectively.

4.3.3. CH_3 vibrations

The AMPMA possesses three CH_3 groups. There are nine fundamentals, namely the CH_3 symmetrical stretching and CH_3 asymmetric stretching, CH_3 symmetrical deformation and CH_3 asymmetrical deformation modes; in-plane stretching and out-of-plane stretching modes; out-of-plane rocking (CH_3opr), twisting (tCH_3) modes and the CH_3 in-plane rocking (ipr) for CH_3 vibrations. Methyl groups are stated as an electron donor substitution and the methyl C–H stretching vibrations lie in the limit, 2975–2840 cm^{-1}.

The IR and Raman modes observed at 1406 cm^{-1} and 1409 cm^{-1} are attributed to in-plane CH bending vibrations. These fundamentals are better coincidence with the values calculated by B3LYP and HF methods.

4.3.4. C-O vibrations

The performance C-O vibrations can be studied through the oxygen lone pair electron. These multiple bonded groups are highly polar and resulting in a strong IR absorption peak. The intermolecular hydrogen bond across C and O diminishes the frequencies of C=O stretching (abs.) due to the different electronegativity of carbon and oxygen as well as the unequal distribution of the bond distance between the two atoms. The electron lone pair of oxygen reveals the nature of the carbonyl group. The carboxylic acid, C=O band reveals a strong absorption within the limit,1700-1800 cm^{-1}. C=O stretching modes of acid are stronger than ketonic C=O bands.

The characteristic ketonic frequency of C=O appears at 1728 cm^{-1} in FTIR and 1745 cm^{-1} in FT-Raman with very weak intensities. This C=O vibration observed is not altered by other bands. The theoretically estimated frequencies by B3LYP *(6-311++G(d,p))* for C=O are 1743

and 1726 cm^{-1} which gives, strong support to the experimental data. However the HF method gives this vibration at higher wavenumbers.

The C–O stretching vibrations are observed at 1215 & 1056 cm^{-1} in FT-Raman and FT-IR, the corresponding bands (C–O stretching) are located at 1195, 1065 and 1040 cm^{-1}. The computed values of C–O stretching are appeared at 1213, 1192, 1093 and 1035 cm^{-1} in *B3LYP (6-311+G(d,p)* and 1235, 1214, 1099 and 1075 cm^{-1} in *B3LYP (6-311+G(d,p)* methods.

4.4. NMR spectral analysis

NMR spectra provide efficient structural information and $^{1}H/^{13}C$ NMR spectra of AMPMA are provided in Fig. **SM 2 (Supplementary Material)**. Theoretically predicted and experimentally identified NMR chemical shifts are shown in Table 3. The chemical shift of ^{1}H and ^{13}C were estimated using IEFPCM/$CDCl_3$ solution. CH_3 and CH_2 proton NMR values of AMPMA appeared from 2 to 1 ppm except for H22. The H22 NMR value slightly deviates due to the nearest oxygen (O28) atom. Methyl protons devoted to the carbonyl group produced their signals at 2.112 ppm and hence they are chemically equivalent. The methyl protons devoted to the phenyl ring give their signals at 2.45 ppm. The phenyl ring proton NMR appears in the range 8.5 to 6.5 ppm. In our compound, the NMR values of H3, H5, H7 and H9 confirm their position with experimental values. One proton of acetoxy group produces its signal at 7.20 ppm. Chemical shift observed at 7.83 ppm is attributed to meta protons of phenyl and at 7.51 ppm is due to Orthoprotons of phenyl. The solvent ($CDCl_3$) peak appears at 7.26 ppm.

^{13}C NMR spectrum gives the carbon environment in the molecule. Carbonyl carbon atoms give their peak at 134.17 ppm. Acetoxy carbon gives its peak at 139.19 ppm. The carbon atom attached to the acetoxy group is attributed to 129.68 ppm. Meta C-atoms of phenyl shows at 129.19 ppm and ortho C-atoms of phenyl ring shows at 126.44 ppm. The methyl group carbon

atom (CH_3) attached to the phenyl ring gives its peak at 105.24 ppm. The medium peak at 14.56 ppm is attributed to the three equivalent CH_3 groups. The triplet (77.49, 77.06 and 76.64 ppm) is owing to the solvent ($CDCl_3$) effect.

4.5. Ultraviolet (UV) spectral analysis and Frontier molecular orbitals (FMOs)

UV spectral studies of AMPMA were demonstrated theoretically with DMSO, chloroform and gas respectively. Low-lying excited levels of AMPMA were obtained by *TD-DFT/B3LYP/6-311++G(d,p)* calculations with the use of fully optimized structure. The theoretical values of oscillator strengths, electronic excitation energies and wavelength are provided in Table 4. From the Table 4, it is noted that the estimated absorption maxima were found to be 241.29, 218.93, 211.95, 210.58 and 206.99 nm for gas phase, 241.42, 219.24, 212.18, 210.78 and 207.42 nm for DMSO and 241.61, 219.64, 213.04, 211.65 and 207.55 nm for chloroform at *DFT/B3LYP/6-311++G(d,p)* method. The maximum contribution to the transitions was chosen with the help of a SWizard program [26]. The maximum absorption of 65% in all three media is due to the electron shift between HOMO and LUMO. The estimated excitation energies, wavelength and oscillator strength with major assistances are provided in Table 4.

The FMOs play an important part in quantum chemistry, optical and electrical analysis [27]. Gauss-Sum 2.2 Program [28] was utilized to estimate the frontier orbital energy and the energy gap of HOMO-LUMO which involved in the estimation of kinetic stability, chemical reactivity, chemical hardness/softness of a molecule and optical polarizability. Chemical hardness and softness are the tools in the clarification of thermodynamic characteristics of chemical reactivity. The plot of the density of states is presented in Fig. 6. It gives the

information about the population study per orbital and establishes a modest molecular orbital view in a definite energy range.

From the FMO energy states of the AMPMA, it is noticed that the respective electronic transfer has occurred between HOMO and LUMO, HOMO-1 and LUMO+1 orbitals, respectively. There are four significant molecular orbitals were found for AMPMA: the highest, second highest occupied (HOMO, HOMO−1), the lowest unoccupied and the second lowest unoccupied (LUMO and LUMO+1) orbitals were estimated using *B3LYP/6-311++G(d,p)* and the estimated energy values are compiled in Table 5. The energy gap value is 6.0260, 6.0233 and 6.0222 eV in gas, DMSO and chloroform respectively. Charge transfer interactions within the molecule can be studied by the energy band gap value of HOMO–LUMO.

Fig. 7 shows the HOMO/LUMO 3D plot of AMPMA and from this figure, one can understand that the highest occupied molecular orbital is localized the entire molecule, particularly on the rings. LUMO is localized at the oxygen atom sites and the aromatic ring. The positive and negative regions are indicated by the red and green colors respectively and the electron density transfer can be identified by the HOMO→LUMO transition.

The values of electronegativity (4.0473 eV), chemical hardness (3.0310 eV), softness (0.1659 eV) and electrophilicity index (1.5065 eV) in the gas stage are greater than that in DMSO and chloroform phases. Larger the dipole moment indicates stronger the intermolecular interactions in the compound. Table 5 reveals the estimated dipole moment values of the molecule. It is observed from the table that the estimated dipole moment is higher for the gas phase (3.7101 D) when compared to DMSO (3.6929 D) and Chloroform (3.4123 D) respectively.

4.6.Thermodynamic properties

According to *B3LYP/6-311++G(d,p)* level, the statistical thermodynamic factors like heat

capacity (*C*), entropy (*S*) and enthalpy changes (*ΔH*) for AMPMA were calculated and are given in Table 6. These thermodynamic parameters are increased in the temperature region, 100- 500 K. It is because, with the increase of temperature, the intensity of molecular vibrations is increased [29].

The correlation equations connecting, enthalpy changes, entropies, heat capacities and temperatures were close-fitting with the quadratic formulas. The respective fitting factors (R^2) for the mentioned thermodynamic components are having the same value 0.9999. The corresponding fitting equations are as follows and the correlation graphics are presented in Fig. 8.

$$S = 59.14269 + 0.29269\,T - 0.3303\,x10^{-4}\,T^2$$

$$\Delta H = -0.25043 + 0.01448\,T + 7.75478\,x10^{-5}\,T^2$$

$$C = 11.80259 + 0.16338\,T - 1.6857\,x10^{-5}\,T^2$$

All the thermodynamic data provides sufficient details which could be helpful for further analysis. They will be used for the other thermodynamic energy calculations within the thermochemical field.

Note: All the thermodynamic estimations were analyzed by choosing the gas phase and are not suitable for the solution phase.

4.7. Electrostatic potential analysis of AMPMA

Fig. **SM 3 (Supplementary Material)** represents the 3D-photograph of ESP-electrostatic potential, TED-total electron density and MEP-molecular electrostatic potential map of AMPMA. The TED photograph of AMPMA molecule shows its identical distribution. However, it is observed from the ESP that the yellowish blob represents the localization of ESP with the oxygen atoms of the molecule. This is the expected result, since ESP associates with

electronegativity and limited charges.

Proton attraction by the high electron density reveals negative electrostatic potential which is red on the ESP surface and the repulsion of the proton by the low electron density shows the positive electrostatic potential and the shades of blue color exhibits the incomplete shielding of nuclear charge. However, the color grading of MEP displays molecular shape, size, positive, negative and neutral ESP regions respectively (Fig. **SM 3**) and thus the physiochemical properties of the molecule can be easily studied [30-32]. Different color identifies the diverse estimations of ESP at the molecular surface.

Potential increases in the order red < orange < yellow < green < blue. The color code of these maps is in the range between -0.04671 a.u. (deep red) to 0.04671 a.u. (Deep Blue), where the strong attraction and repulsion behavior of the molecule are indicated by blue and red colors respectively. In the MEP map, the ring carbon and O-atoms of the molecule indicate the negative potential region whereas the hydrogen atoms in the network indicate the positive potential. The green colour of the methyl groups present dictates the neutral potential.

4.8. Natural Bond Orbital(NBO) analysis

The NBO analysis evidenced to be an important measure of interpretation of intra and intermolecular interaction. It is also used for examining conjugative contact or charge transfer with the molecular system. Higher the energy of hyper conjugative interactions, the more severe is the interface between electron donors and acceptors respectively.

The delocalization of electron density, intramolecular interactions and re-hybridization of the molecule can be understood through NBO analysis. Fock-second order perturbation theory examination on AMPMA molecule is provided in Table **SM 3 (Supplementary Material)**. The intramolecular interactions of the molecule could be owed to the orbital overlap of π(C6-C8)

over anti-bonding π^*(C1-C10) and π^*(C2-C4) with energies 18.12 kcal/mol and 21.6 kcal/mol, π(C1-C10) and π(C2-C4) over π^*(C6-C8) with stabilization energies 21.81 kcal/mol and 18.61 kcal/mol. The molecule involves the interactions of σ of O25 with σ^*(C12-O26), σ of O26 with σ^*(C12-O25), σ of O27 with σ^*(C11-C28) and σ of O28 with σ^*(C17-C27) and has stabilization energies 6.94 kcal/mol, 1.28 kcal/mol, 7.05 kcal/mol and 1.39 kcal/mol, respectively.

4.9. Optical properties

4.9.1. Molecular dipole moment and polarizability calculations

Observation of optical activity in organic molecules provides the necessary key factors for most of the optical properties like optical switching, optical modulation, optical logic and signal processing etc., [33-36]. It is believed that in most of the organic materials, intramolecular interactions are much tougher than the intermolecular chemical bonds. In such circumstances, the molecular interactions of AMPMA were analyzed with different theoretical methods (MP2, DFT and HF).

The optical activity of the materials significantly depends on large dipole moment and polariability. The aromatic ring in the titled material is responsible for all the optical properties. When an optical photons incident on the material, there is a transfer of energy to the electrons and thus there is a development of the local electric field. Therefore, in this contest, the calcualtion of the optical properties like molecular dipole moment (μ) and linear polarizability (α) of AMPMA were studied by MP2, DFT and HF methods with different basis sets.

In the present research work, the axial components of molecular dipole moment (μ) and polarizability (α) were calculated along the axial planes (x, y and z respectively). In addition to these axial components, the methods were extended to describe the non axial components (*xy*, *xz*,

yz) of an applying electric field apart from the axial planes. The polarizability tensors were estimated (α_{xx}, α_{xy}, α_{yy}, α_{xz}, α_{yz}, α_{zz}) by using the Gaussian output file with an appropriate formula [37] and the results based on *DFT/B3LYP 6-311++g(d,p)* method are recorded in Table 7. The dipole moment (μ) and polarizability (α) of the AMPMA material are compared with the reported materials and are presented in Table 8. The larger values of dipolemoment (μ) and polarizability (α) indicate the substantial charge delocalization in the mentioned directions, which shall responsible for the nonlinear optical activity.

4.9.2. Basis sets analysis of DFT, MP2 and HF methods

It is noted from Fig. 9, the estimated electrostatic dipole moments from all the three methods are having a similar trend. This reveals that the dipole moments were insensitive to electrostatic correlation effect (EC) [41]. In all the three methods, *6-31+g(d,p) and 6-31++g(d,p)* basis set gives maximum dipole moment and the basis set of *6-311g(d,p)* shows the minimum dipole moment value. The results of MP2 method having 22% deviation from HF method and it is 15% from DFT.

The polarizability behavior of the molecule can be understood from Fig. 10. The behavior of the curves in all three methods revealed the molecular consistency in the estimation of linear polarizability. Large the value of polarisability, more diffusion and polarization functions will be considered [41]. In the DFT scheme, the obtained polarisability values are in the region from 19 $x10^{-24}$ esu to 22 $x10^{-24}$ esu. The *6-31+g(d,p)* and *6-31++g(d,p)* basis sets in DFT approach showed maximum values of polarizabilities and hence these basis sets are suitable for theoretical calculations.

5. Conclusion

A complete chemical computational analysis of AMPMA was performed by *HF* and *DFT-B3LYP* method at *6-311++G(d,p)* basis level. An experimentally obtained and theoretically generated spectra were well granted for the decent frequency fit with *DFT B3LYP/6-311++G(d,p)* level. The structural and symmetrical properties of AMPMA were studied with various quantum chemical calculations. UV-Vis. spectral studies of AMPMA were analyzed by theoretical calculations. The electronic transitions of the material were completely studied by the DFT method both with the gas phase and liquid phase (solvent-DMSO and Chloroform) respectively. The MEP map explains the negative (oxygen and nitrogen atoms) and positive (hydrogen atoms) potentials. Different theoretical approaches on different basis sets were used to analyze the dipole moment and polarisability of the title molecule. The higher values of dipole moment and polarisability components of the titled material dictates the considerable charge delocalization which is accountable for its efficient optical property.

Acknowledgements

The author Dr. N. Sivakumar wish to acknowledge UGC (Dr.S.Kothari Postdoctoral Research scheme. No.F.4-2/2006/(BSR)/PH/16-17/0109), New Delhi for proving the financial assistance to carried out this research work.

References

[1] G.E. Negrón, L.N. Palacios, D. Angeles, L. Lomas, R. Gaviño, A mild and efficient method for the chemoselective synthesis of acylals from aromatic aldehydes and their deprotections catalyzed by sulfated zirconia, J. Braz. Chem. Soc. 16 (2005) 490-494. doi: 10.1590/S0103-50532005000300025.

[2] B.M.Trost ,C. Lee , *gem*-Diacetates as Carbonyl Surrogates for Asymmetric Synthesis. Total Syntheses of Sphingofungins E and F, J. Am. Chem. Soc. 123 (2001) 12191-12201. doi: 10.1021/ja0118338.

[3] M. Sandberg, L.K. Sydnes, The Chemistry of Acylals. 3. Cyanohydrin Esters from Acylals with Cyanide Reagents, Org. Lett. 2 (2000) 687-689. doi:10.1021/ol005535b.

[4] F.R. Van Heerden, J.J. Huyser, D. Bradley, G. Williams, C.W. Holzapfel, Palladium catalysed substitution reactions of *geminal* allylic diacetates, Tetrahedron Lett. 39 (1988) 5281-5284. doi:10.1016/S0040-4039(98)01000-4.

[5] M. Sandberg, L.K. Sydnes, The chemistry of acylals. Part II. Formation of nitriles by treatment of acylals with trimethylsilyl azide in the presence of a Lewis acid, Tetrahedron Lett. 39 (1998) 6361-6364. doi: 10.1016/S0040-4039(98)01309-4.

[6] J. G. Frick Jr, R.J. Harper Jr, Acetals as crosslinking reagents for cotton, J. Appl. Polym. Sci. 29 (1984) 1433-1447. doi: 10.1002/app.1984.070290436.

[7] W. R. Sanderson, Eur. Pat. Appl., EP. 125 (1984) 781 (*Chem. Abstr.*102, p64010k).

[8] J. Kanchanadevi, G. Anbalagan, V. Saravanan, A. K. Mohanakrishnan , V. Manivannan, (Acetoxy)(2-methylphenyl)methyl acetate, ActaCryst. E 67 (2011), o2111. doi: 10.1107/S1600536811028625.

[9] Farhad Shirini, Nader Ghaffari Khaligh, A succinimide-*N*-sulfonic acid catalyst for acetylation reactions in absence of a solvent, Chin. J. Catal. 34 (2013) 695–703. doi: 10.1016/S1872-2067(11)60499-3.

[10] Rajnikant, Lovely Sarmal, Kamni, Dinesh, M.B. Deshmukh, Synthesis and X-ray structure of 1-acetoxy 4-methylphenyl methyl acetate J. Chem. Crystallogr. 39 (2009) 835-837. doi: 10.1007/s10870-009-9576-2.

[11] M. J. Frisch, G. W. Trucks, H. B. Schlegel, G. E. Scuseria, M. A. Robb, J. R. Cheeseman, G. Scalmani, V. Barone, G. A. Petersson, H. Nakatsuji, X. Li, M. Caricato, A. Marenich, J. Bloino, B. G. Janesko, R. Gomperts, B. Mennucci, H. P. Hratchian, J. V. Ortiz, A. F. Izmaylov, J. L. Sonnenberg, D. Williams-Young, F. Ding, F. Lipparini, F. Egidi, J. Goings, B. Peng, A. Petrone, T. Henderson, D. Ranasinghe, V. G. Zakrzewski, J. Gao, N. Rega, G. Zheng, W. Liang, M. Hada, M. Ehara, K. Toyota, R. Fukuda, J. Hasegawa, M. Ishida, T. Nakajima, Y. Honda, O. Kitao, H. Nakai, T. Vreven, K. Throssell, J. A. Montgomery, Jr., J. E. Peralta, F. Ogliaro, M. Bearpark, J. J. Heyd, E. Brothers, K. N. Kudin, V. N. Staroverov, T. Keith, R. Kobayashi, J. Normand, K. Raghavachari, A. Rendell, J. C. Burant, S. S. Iyengar, J. Tomasi, M. Cossi, J. M. Millam, M. Klene, C. Adamo, R. Cammi, J. W. Ochterski, R. L. Martin, K. Morokuma, O. Farkas, J. B. Foresman, and D. J. Fox, Gaussian 09, Revision A.02, Gaussian, Inc., Wallingford CT, 2016.

[12] D.C. Young, Computational Chemistry: A Practical Guide for Applying Techniques to Real World Problems (Electronic), John Wiley & Sons Inc., New York, 2001.

[13] M. Karabacak, A. Coruh, M. Kurt, FT-IR, FT-Raman, NMR spectra, and molecular structure investigation of 2,3-dibromo-*N*-methylmaleimide: A combined experimental and theoretical study, J. Mol. Struct. 892 (2008) 125-131. doi: 10.1016/j.molstruc.2008.05.014.

[14] N. Sundaraganesan, S. Illakiamani, H. Saleem, P.M. Wojciechowski, D. Michalska, FT-Raman and FT-IR spectra, vibrational assignments and density functional studies of 5-bromo-2-nitropyridine, Spectrochim. Acta A 61 (2005) 2995-3001. doi:10.1016/j.saa.2004.11.016.

[15] A. Frisch, A.B. Nielsen, A.J. Holder, Gaussview Users Manual, Gaussian Inc., Pittsburg, 2003.

[16] R.I. Dennington, T. Keith, J. Millam, K. Eppinnett, W. Hovell, Gauss View Version 5, 2009.

[17] G. Keresztury, S. Holly, G. Besenyei, J. Varga, A.Y. Wang, J.R. Durig, Vibrational spectra of monothiocarbamates-II. IR and Raman spectra, vibrational assignment, conformational analysis and ab initio calculations of S-methyl-N, N-dimethylthiocarbamate, Spectrochim. Acta A 9 (1993) 2007-2026. doi: 10.1016/S0584-8539(09)91012-1.

[18] G. Keresztury, in: J.M. Chalmers, P.R. Griffith (Eds.), Raman Spectroscopy: Theory, Hand book of Vibrational Spectroscopy, vol. 1, John Wiley & Sons Ltd., New York, 2002.

[19] V. Krishnakumar, R.J. Xavier, Normal coordinate analysis of 2-mercapto and 4,6-dihydroxy -2-mercapto pyrimidines, Indian J. Pure Appl. Phys. 41 (2003) 597-601. ISSN: 00195596

[20] A. Srivastava, V.B. Singh, Theoretical and experimental studies of vibrational spectra of naphthalene and its cation, Indian J. Pure Appl. Phys. 45 (2007) 714-720. ISSN:00195596

[21] D. Lin–Vien, N.B. Colthup, W.G. Fateley, J.G. Grasselli, The Handbook of Infrared Raman Characteristic Frequencies of Organic Molecules, Academic Press, Boston, MA, 1991.

[22] M. Karabacak, C. Karaca, A. Atac, M. Eskici, A. Karanfil, EtemKose, Synthesis, analysis of spectroscopic and nonlinear optical properties of the novel compound: (S)-N-benzyl-1-phenyl-5-(thiophen-3-yl)-4-pentyn-2-amine, Spectrochim. Acta A 97 (2012) 556-567. doi: 10.1016/j.saa.2012.05.087.

[23] Diwaker, C. S. Chidan Kumar, Ashish Kumar, Siddegowda Chandraju, Hoong-Kun Fun, Synthesis, Spectroscopic characterization, electronic and optical studies of (2Z)-5,6-dimethyl-2-[(4-nitrophenyl)methylidene]-2,3-dihydro-1-benzofuran-3-one, J. Comput. Sci. 10 (2015) 237-246. doi: 10.1016/j.jocs.2014.11.005.

[24] A.K. Mishra, DFT study of structural, vibrational and electronic properties of polyaniline pernigraniline model compounds, J. Comput. Sci. 10 (2015) 195-208. doi: 10.1016/j.jocs.2015.02.003.

[25] X. Zhang, Q. Zhou, Y. Huang, Z. Li, Z. Zhang, Constructive analysis of the Raman spectra of Polychlorinated Benzene: Hexachlorobenzene and Benzene, Sens. 11, (2011) 11510-11515. doi:10.3390/s111211510

[26] S.I. Gorelsky, SWizard Program Revision 4.5, http://www.sg.chem.net/, University of Ottawa, Ottawa, Canada, 2010.

[27] I. Fleming, Frontier Orbitals and Osrganic Chemical Reactions, Wiley, London, 1976.

[28] N.M.O' Boyle, A.L. Tenderholt, K.M. Langer, cclib: A library for package□independent computational chemistry algorithms, J. Comput. Chem. 29 (2008) 839-845. doi: 10.1002/jcc.20823.

29] J. Bevan Ott, J. Boerio-Goates, Calculations from Statistical Thermodynamics, Academic Press, 2000.

[30] J.S. Murray, K. Sen, Molecular Electrostatic Potentials, Concepts and 399 Applications, Elsevier, Amsterdam, 1996.

[31] E. Scrocco, J. Tomasi, in: P. Lowdin (Ed.), Advances in Quantum Chemistry, Academic Press, New York, 1978.

[32] J. Sponer, P. Hobza, DNA base amino groups and their role in molecular interactions: Ab initio and preliminary density functional theory calculations, Int. J. Quant. Chem. 57 (1996) 959-970. doi: 10.1002/(SICI)1097-461X(1996)57:5<959::AID-QUA16>3.0.CO;2-S

[33] C. Andraud, T. Brotin, C. Garcia, F. Pelle, P. Goldner, B. Bigot, A. Collet, Theoretical and experimental investigations of the nonlinear optical properties of vanillin, polyenovanillin, and bisvanillin derivatives, J. Am. Chem. Soc. 116 (1994) 2094-2102. doi: 10.1021/ja00084a055.

[34] V.M. Geskin, C. Lambert, J.L. Bredas, Origin of High Second- and Third-Order Nonlinear Optical Response in Ammonio/Borato Diphenylpolyene Zwitterions: the Remarkable Role of Polarized Aromatic Groups, J. Am. Chem. Soc. 125 (2003) 15651-15658. doi: 10.1021/ja035862p.

[35] N. Sivakumar, J. Srividya, J. Mohana, G. Anbalagan, Growth, crystalline perfection, spectral and optical characterization of a novel optical material: l-tryptophan p-nitrophenol trisolvate single crystal, Spectrochim. Acta A 139 (2015) 156-164. doi: 10.106/j.saa.2014.12.044.

[36] D.F. Eaton, Nonlinear optical materials, Science 25 (1991) 281-287. doi: 10.1126/science.253.5017.281.

[37] X. Liu, Y. Su, M. Ren, Theoretical investigations of optical properties of l-arginine trifluoroacetate crystal, Mater. Chem. Phys. 142, 2013, 286-291. doi: 10.1016/j.matchemphys.2013.07.016.

[38] S.P. Vijayachamundeeswari, B. Yagna Narayana, S. Jone Pradeepa, N. Sundaraganesan, Vibrational analysis, NBO analysis, NMR, UV-VIS, hyperpolarizability analysis of Trimethadione by density functional theory, J. Mol. Struct. 1099 (2015) 633-643 doi: 10.1016/j.molstruc.2015.06.079

[39] K. Govindarasu, E. Kavitha, Molecular structure, Vibrational spectra, NBO, UV and first order Hyperpolarizability, analysis of 4-Chloro-DL-phenylalanine by Density Functional Theory, Spectrochim. Acta 133 (2014) 799-810. doi: 10.1016/j.saa.2014.06.019.

[40] V. Karunakaran a, V. Balachandran, Experimental and theoretical investigation of the molecular structure, conformational stability, hyperpolarizability, electrostatic potential, thermodynamic properties and NMR spectra of pharmaceutical important molecule:4'-Methylpropiophenone, Spectrochim. Acta 128 (2014) 1–14. doi: 10.1016/j.saa.2014.02.155.

[41] Y.X. Sun, Q.L. Hao, W.X. Wei, Z.X. Yu, L.D. Lu, X. Wang, Y.S. Wang, Experimental and density functional studies on 4-(3,4-dihydroxybenzylideneamino) antipyrine, and 4-(2,3,4-trihydroxybenzylideneamino) antipyrine, J. Mol. Struct. Theochem. 904 (2009) 74-82. doi: 10.1016/j.theochem.2009.02.036.

Table 1. Crystal data, Intensity data collection and Refinement for methyl acetate compound AMPMA.

PARAMETERS	**AMPMA**
CRYSTAL DATA	
Formula	$C_{12}\ H_{14}\ O_4$
Formula Weight	222.23
Crystal System	Monoclinic
Space group	*C2/c*
a, b, c [Å]	15.757(5) 7.564(5) 19.886(5)
alpha, beta, gamma [deg]	90.00 99.17(5) 90.00
V [$Å^3$]	2339.84(18)
Z	8
D(calc) [g/cm^3]	1.2617
Radiation used	MoK_α
Mu(MoK_α) [mm^{-1}]	0.095
Wavelength	0.71073
F(000)	944
Crystal Size [mm]	0.25×0.20×0.15
INTENSITY DATA COLLECTION	
Diffractometer	Brucker Kappa APEXII CCD
Temperature (K)	295
Theta Min-Max [º]	2.1, 26.5
Dataset	-13:19; -9:8, -24:24
Reflection collected	12571
Unique reflections	2414
Reflection with [I > 0.02 σ(I)]	1856
R(int)	0.027
REFINEMENT	
Refinement method	Full matrix least square on F^2
Parameters	149
GooF on F^2	1.045
Final R indices, wR^2	0.041 0.1249
Extinction Correction	None
Min. and Max. Resd. Dens. [$e/Å^3$]	-0.19, 0.20

Table 2. Non-Bonded interactions and possible hydrogen bonds of AMPMA

D-H…A	D-H(Å)	H…A (Å)	D…A (Å)	D-H-A (°)
C7- H7**…**O2[i]	0.9800	2.2830	2.6641	101.92
C9- H9A**…**O4[ii]	0.9800	2.5410	2.656	85.85

Symmetry Code:(i) x, y, z; (ii) -x+1/2, y+1/2, -z+1/2

Table 3. Experimental and Calculated values of ^{1}H and ^{13}C NMR isotropic chemical shifts (with respect to TMS and in $CDCl_3$ solution) of AMPMA

Atom	^{13}C NMR		Atom	^{13}H NMR	
	Experimental	Calculated (B3LYP)		Experimental	Calculated (B3LYP)
C12		177.4	H9	7.83	7.81
C17		176.6	H30	-	7.76
C1		144.7	H5	7.51	7.51
C10	139.14	140.5	H7	7.49	7.47
C4	134.17	134.8	H3	7.31	7.44
C2	129.68	134.7	H22	-	3.27
C8	129.19	133.1	H24	2.45	2.52
C6	126.44	130.7	H15	-	2.30
C11	105.24	92.0	H20	-	2.24
C13	-	21.4	H16	-	2.18
C18	-	21.1	H23	2.11	2.11
C21	14.56	19.9	H29	-	1.98
			H14	-	1.79
			H19	-	1.60

Table 4. Theoretical electronic absorption spectra of AMPMA (absorption wavelength λ (nm), excitation energies E (eV) and oscillator strengths (*f*) using TD-DFT/B3LYP/6-311++G(d,p) method in DMSO, chloroform and gas phase

Phase	E(eV)	λ(nm)	F(cm^{-1})	Major contribution%
GAS	5.138	241.29	0.0205	HOMO->LUMO (65%)
	5.663	218.93	0.0818	H-1->LUMO (58%)
	5.849	211.95	0.0095	H-3->L+2 (-38%)
	5.887	210.58	0.0005	H-2->L+3 (-63%)
	5.990	206.99	0.0072	HOMO->L+2 (81%)
DMSO	5.135	241.42	0.0219	HOMO->LUMO (65%)
	5.655	219.24	0.0863	H-1->LUMO (58%)
	5.843	212.18	0.0098	H-3->L+2 (-36%)
	5.882	210.78	0.0005	H-2->L+3 (-60%)
	5.977	207.42	0.0067	HOMO->L+2 (82%)
$CHCl_3$	5.131	241.61	0.0220	HOMO->LUMO (64%)
	5.645	219.64	0.0842	H-1->LUMO (56%)
	5.819	213.04	0.0130	H-3->L+2 (-37%)
	5.857	211.65	0.0007	H-2->L+3 (64%)
	5.978	207.55	0.0072	HOMO->L+2 (81%)

Table 5. Calculated HOMO and LUMO energy values of solvents (DMSO and chloroform) and gas phase

Properties	Gas	DMSO	$CHCl_3$
HOMO-1(eV)	-0.5829	-0.5834	-0.5459
HOMO (eV)	-1.0343	-1.0338	-0.9949
LUMO (eV)	-7.0603	-7.0571	-7.0171
LUMO+1 (eV)	-7.2513	-7.2481	-7.2037
HOMO-LUMO (eV)	6.0260	6.0233	6.0222
Electro negativity (χ)	4.0473	4.0454	4.0060
Chemical hardness (η)	3.0130	3.0116	3.0111
Softness (S)	0.1659	0.1660	0.1661
Electrophilicity index (ω)	1.5065	1.5058	1.5056
Dipole moment (Debye)	3.7101	3.6929	3.4123

Table 6.Thermodynamic functions at B3LYP/6- 311++G(d,p)

Temperature (T) (K)	Entropy (S) cal $mol^{-1}K^{-1}$	Enthalpy (ΔH) kcal mol^{-1}	Heat Capacity (Cv) cal $mol^{-1}K^{-1}$
100	87.02	1.96	27.93
150	99.62	3.60	35.66
200	112.57	5.79	43.94
250	123.86	8.19	51.50
300	135.40	11.20	59.61
350	145.40	14.36	67.01
400	154.77	17.88	74.32
450	164.21	22.11	82.16
500	172.28	26.40	89.32

Table 7. The calculated dipole moments (μ, Debye) and polarizability components (α, a.u.) of AMPMA molecule based on B3LYP/6-311++g(d,p) basis level.

Parameters	Values
μ_x	-0.2000
μ_y	-0.5929
μ_z	-0.9146
μ_{tot}	1.1082
α_{xx}	176.4648
α_{xy}	3.9545
α_{yy}	130.3236
α_{xz}	1.8847
α_{yz}	9.0435
α_{zz}	151.4639
α_{tot}	22.6380×10^{-24}esu

Table 8. Comparison of dipole moment (μ, Debye) and polarizability (α, esu) of AMPMA molecule with the reported molecules

Material	Dipole moment (μ, Debye)	Polarizability (α, $\times 10^{-24}$ esu.)	References
Trimethadione	0.8118	10.3001	[38]
4-Chloro-DL-phenylalanine	1.4990	15.5000	[39]
4'-Methylpropiophenone	1.3788	18.1619	[40]
AMPMA	1.1082	22.6380	Present

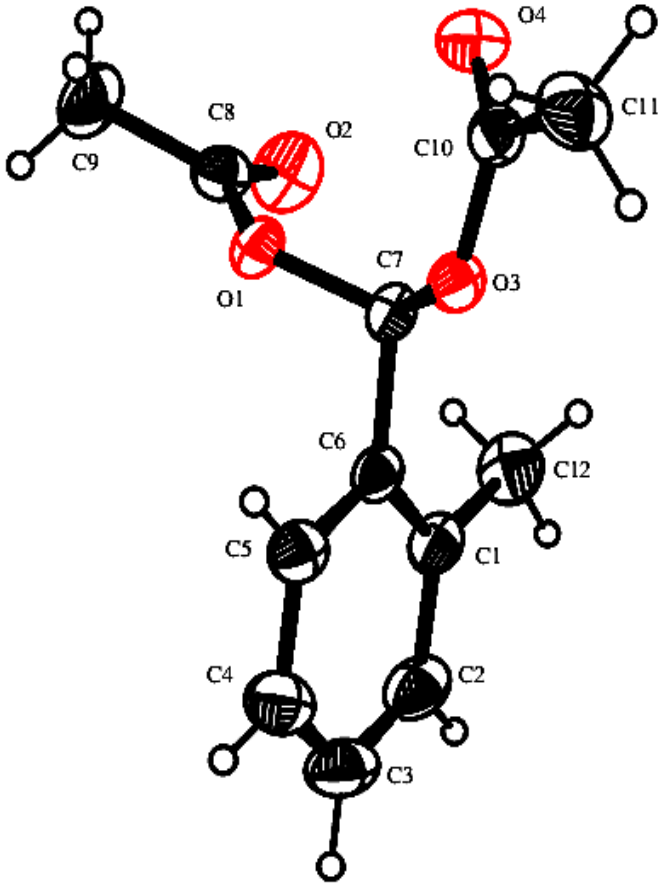

Fig. 1. ORTEP plot of AMPMA drawn at 30% probability of displacement ellipsoids for non-hydrogen atoms

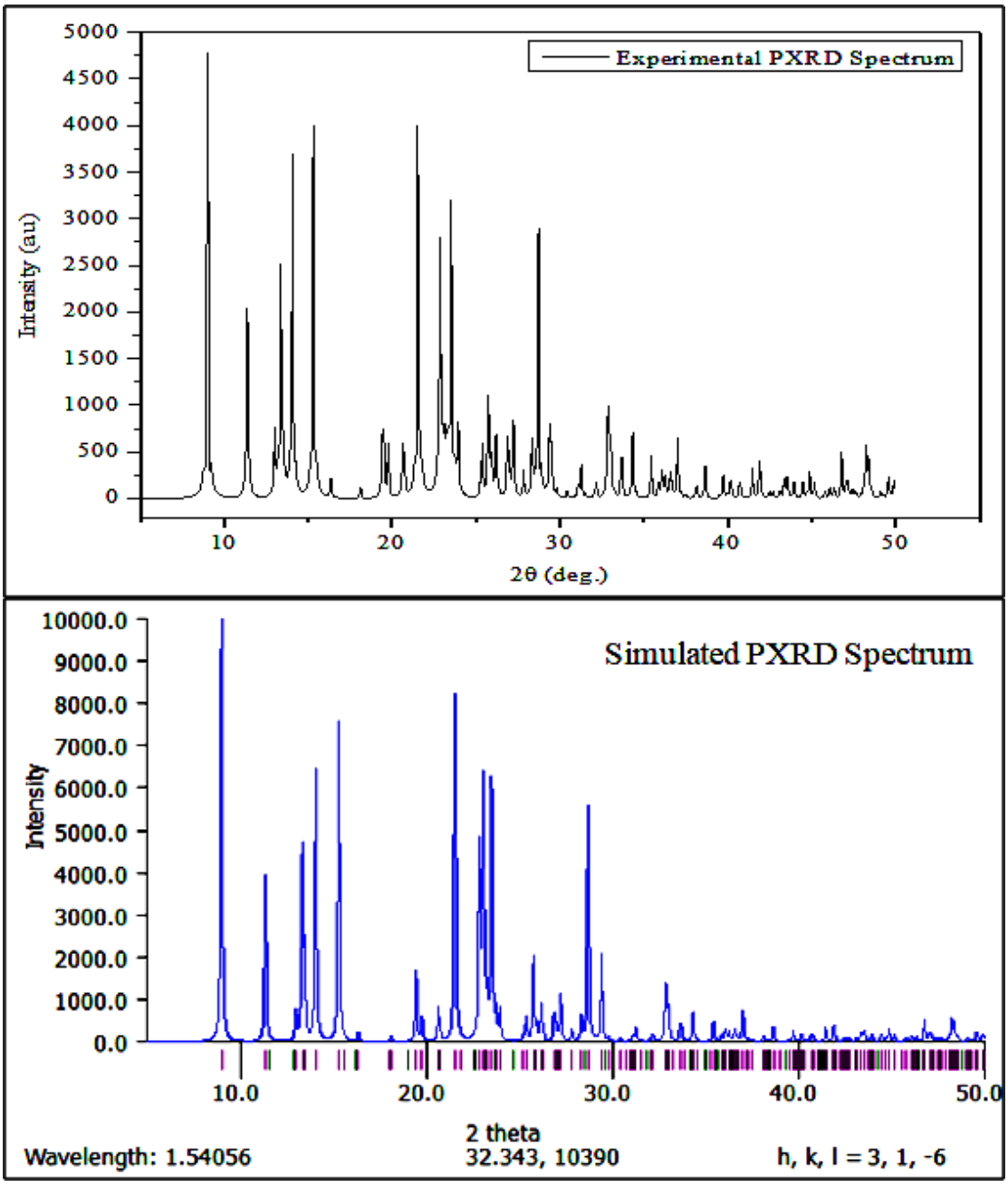

Fig. 2. The simulated and recorded powder X-ray diffraction pattern of the molecule AMPMA

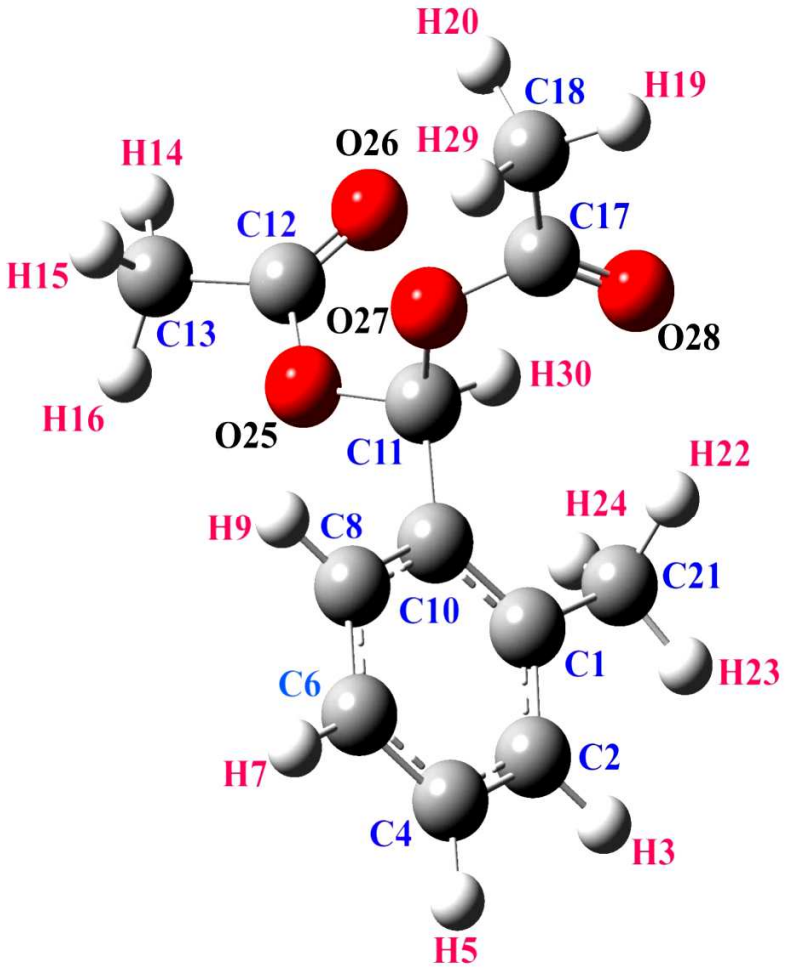

Fig. 3.The optimized molecular structure of AMPMA

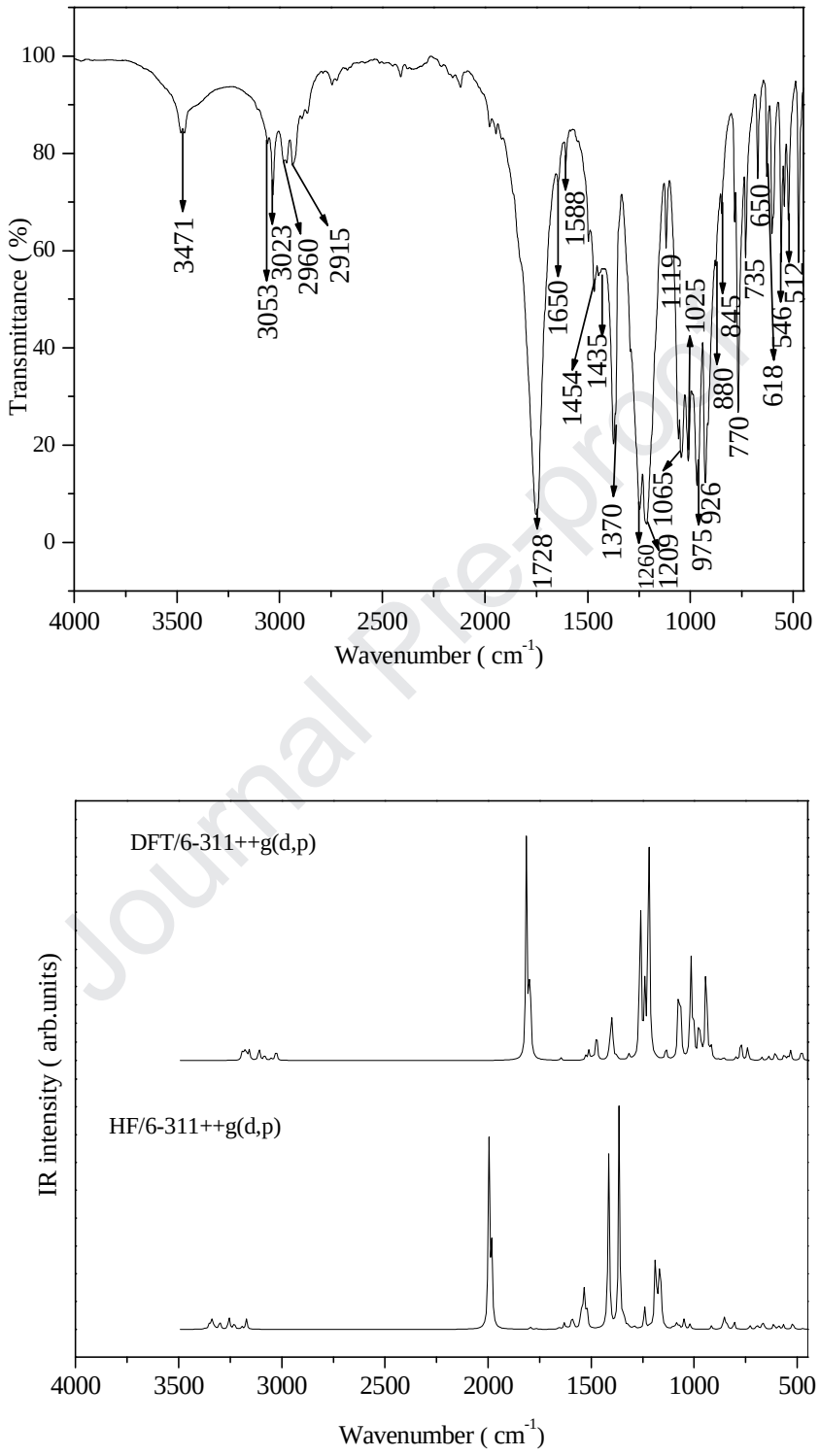

Fig. 4. Experimental and simulated FT-IR spectrum of AMPMA

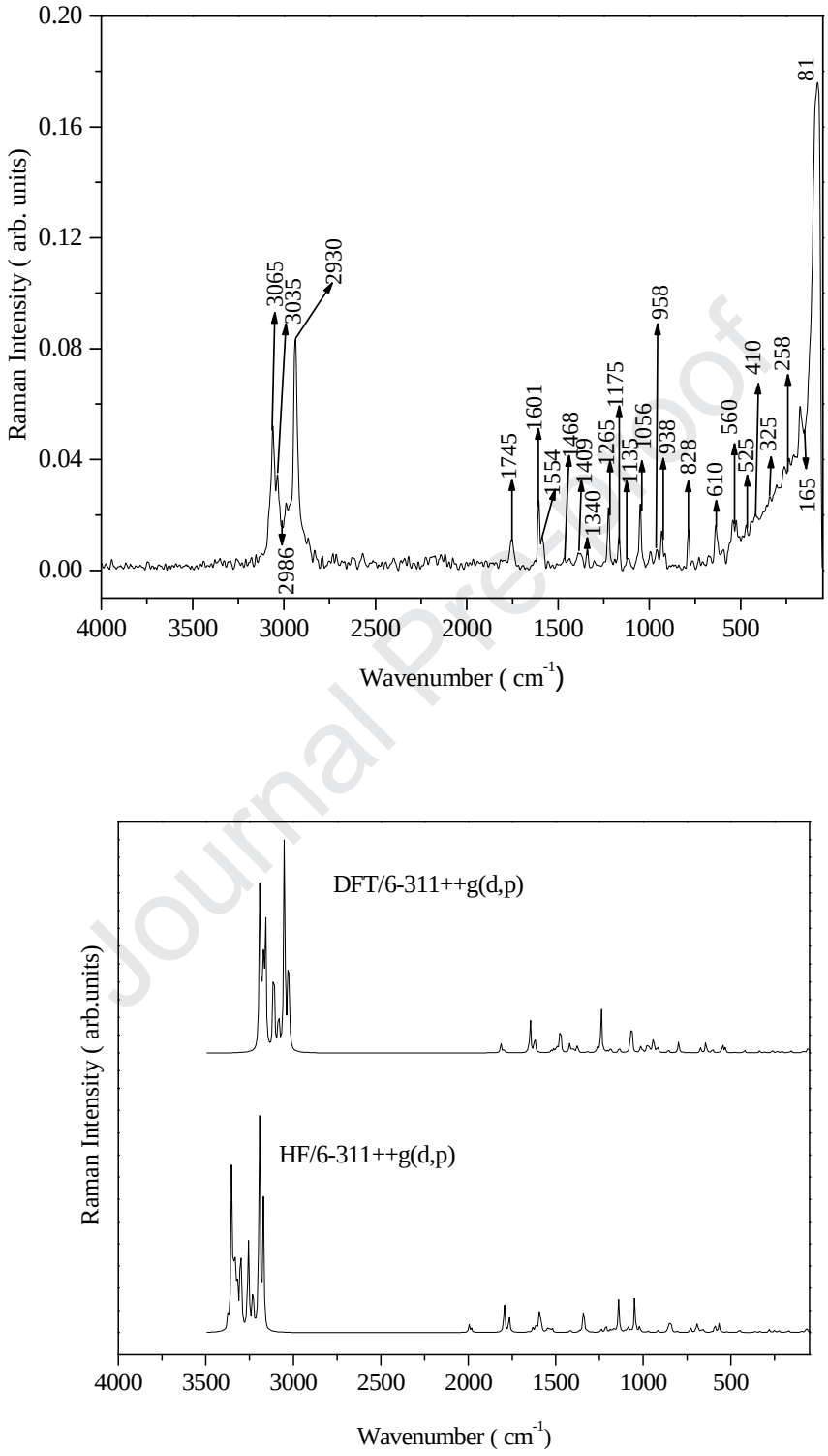

Fig. 5. Experimental and simulated FT-Raman spectrum of AMPMA

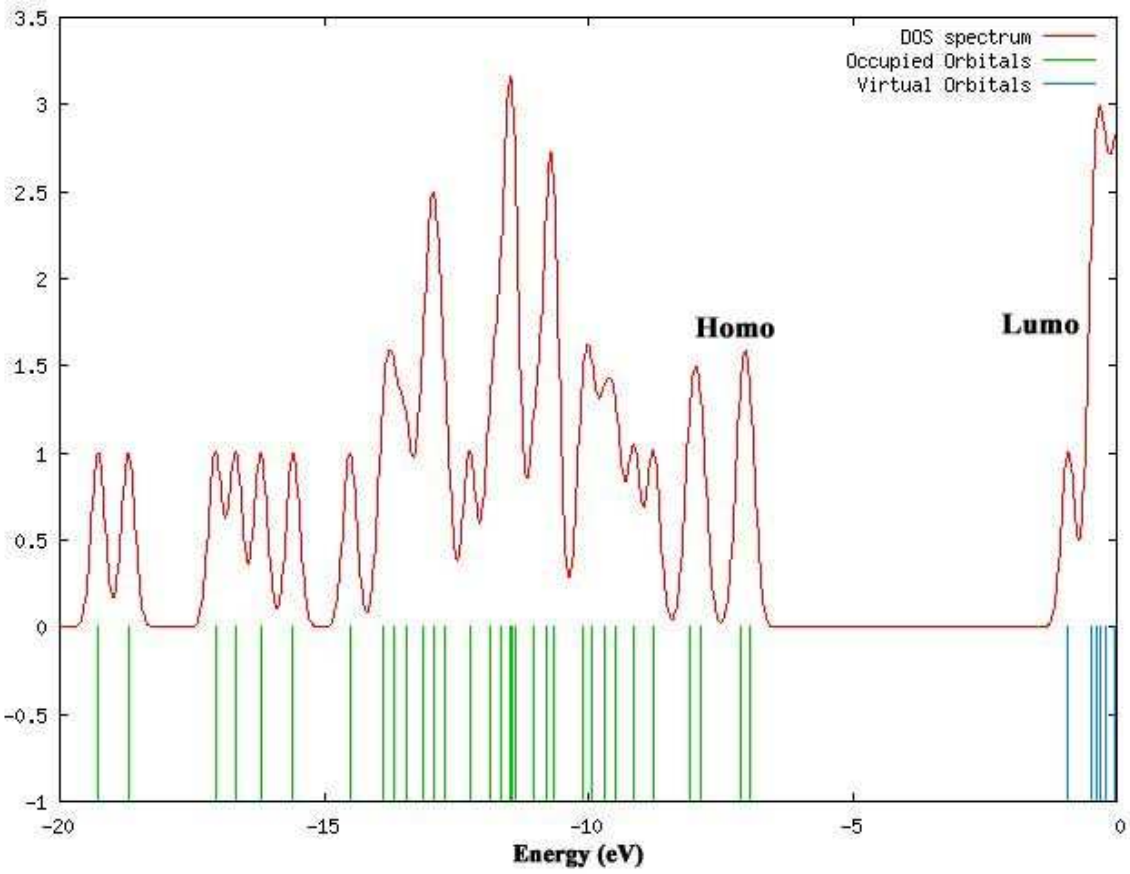

Fig. 6. Density of states (DOS) of AMPMA

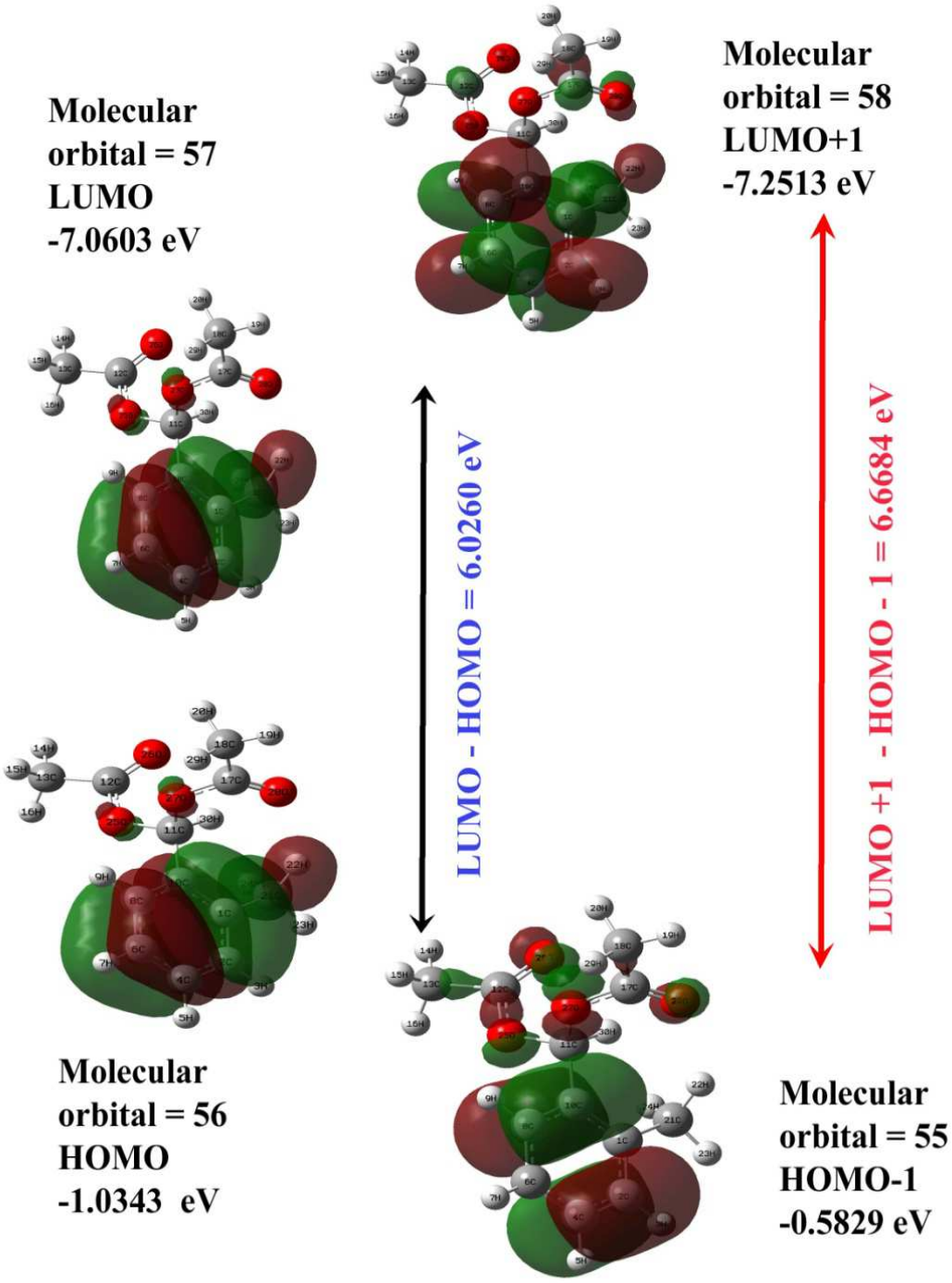

Fig. 7. 3D plots of the HOMO and LUMO orbitals of AMPMA

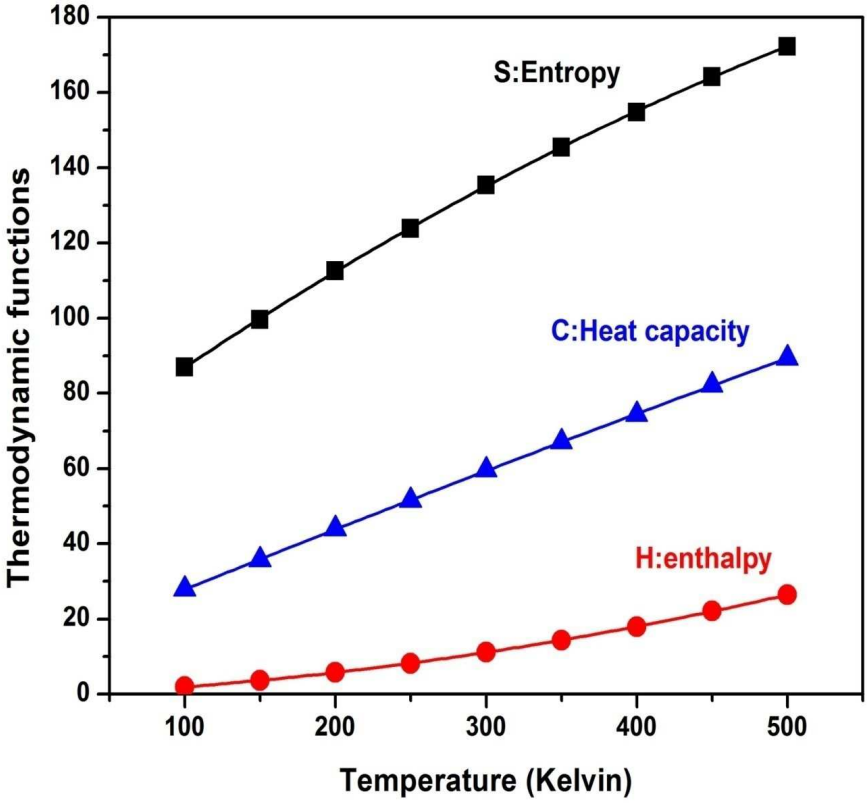

Fig. 8. Variation of thermodynamic properties with temperature (K) of the molecule (AMPMA)

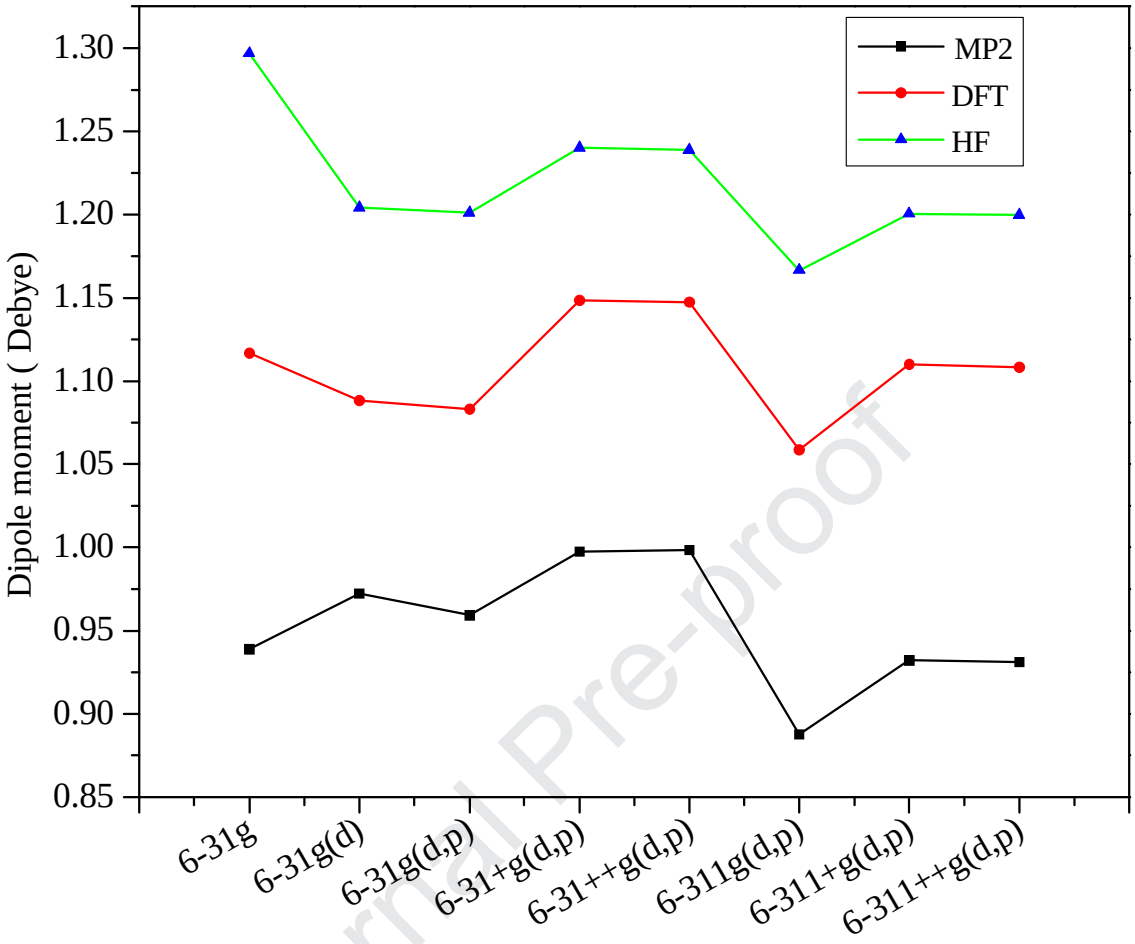

Fig. 9. Dipolemoment of AMPMA with three different methods

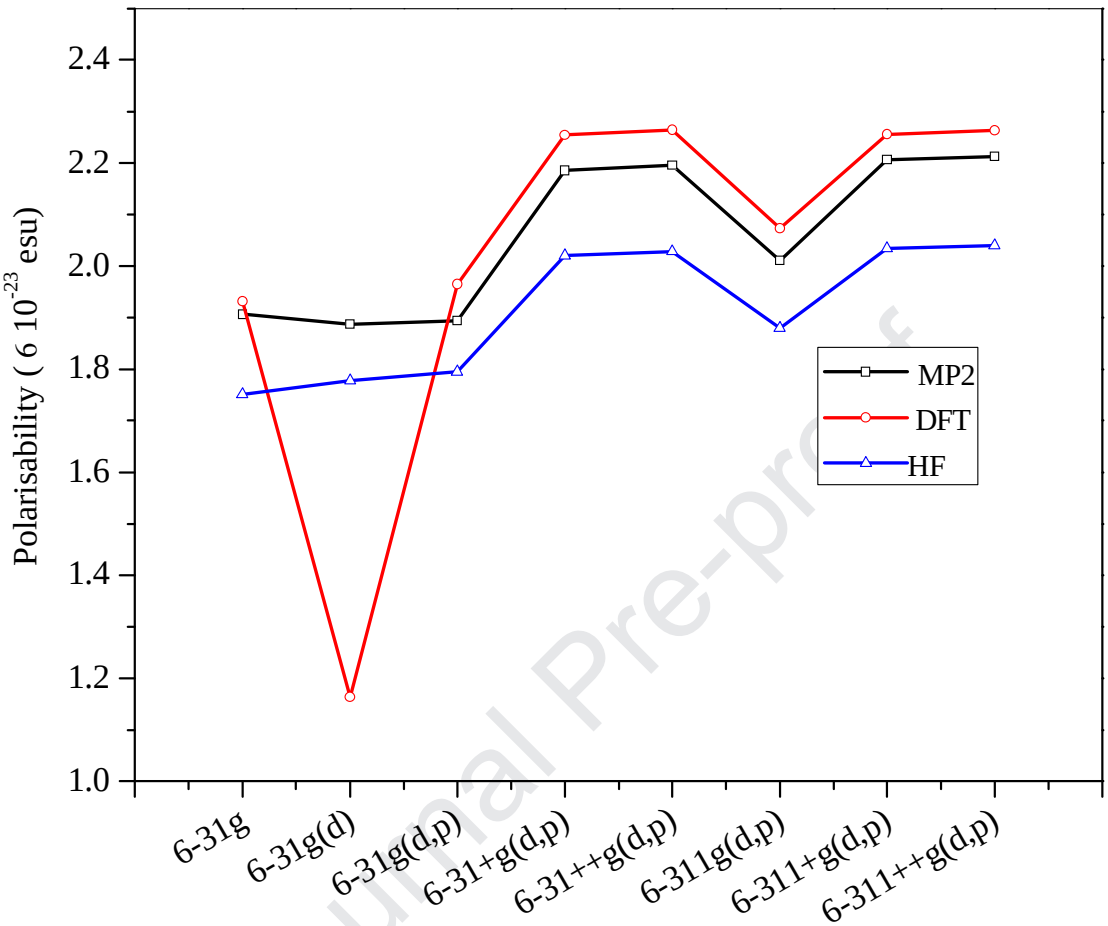

Fig. 10. Polarisability curve of AMPMA with three different methods

Research Highlights

- The molecule AMPMA is theoretically investigated by HF and DFT/B3LYP methods
- Time-Dependent HOMO-LUMO energy is calculated to be 6.0260 eV
- Theoretically estimated value of dipole moment is 1.1082 D
- The polarizability value of AMPMA molecule is found to be 22.6380 $x10^{-24}$ esu
- The elongation and contraction of bond length are responsible for large polarization

Author Statement/Declaration

☐The authors declare that they have no known competing financial interests or personal relationships that could have appeared to influence the work reported in this paper.

☐The authors declare the following financial interests/personal relationships which may be considered as potential competing interests:

The author Dr. N. Sivakumar wish to acknowledge UGC (Dr.S.Kothari Postdoctoral Research scheme), New Delhi for proving the financial assistance to carried out this research work.

The manuscript has not been published previously and it is not under consideration for publication elsewhere, no conflict of interest exists, or if such conflict exists, the exact nature of the conflict must be declared and if accepted. The article will not be published elsewhere in the same form, in any language, without the written consent of the publisher.